BILINGUAL PUBLISHING GROUP

Journal of Building Material Science

https://journals.bilpubgroup.com/index.php/jbms

ARTICLE

Unveiling the Carbonation Behavior and Microstructural Changes of Magnesium Slag at 0 °C

***Junhao Ye*[1], *Songhui Liu*[1*], *Jingrui Fang*[2], *Xuemao Guan*[1], *Hui Guo*[1]**

[1] *Henan Key Laboratory of Materials on Deep-Earth Engineering, School of Materials Science and Engineering, Henan Polytechnic University, Jiaozuo, Henan, 454003, China*

[2] *State Key Laboratory of Green Building Materials, China Building Materials Academy, Beijing, 100024, China*

ABSTRACT

Magnesium slag (MS) is an industrial byproduct with high CO_2 sequestration potential. This study investigates the carbonation behavior and microstructural changes of MS during wet carbonation at 0 °C. XRD, TG, FTIR, SEM, and BET techniques were used to characterize the phase composition, microstructure, and porosity of MS samples carbonated for different durations. The results showed that the main carbonation products were calcite, vaterite, and highly polymerized silica gel, with particle sizes around 1 μm. The low-temperature environment retarded the carbonation reaction rate and affected the morphology and crystallization of calcium carbonate. After 480 min of carbonation, the specific surface area and porosity of MS increased substantially by 740% and 144.6%, respectively, indicating improved reactivity. The microstructure of carbonated MS became denser with calcite particles surrounded by silica gel. This study demonstrates that wet carbonation of MS at 0 °C significantly enhances its properties, creating an ultrafine supplementary cementitious material with considerable CO_2 sequestration capacity.

Keywords: Wet carbonation; Ultrafine supplementary cementitious materials; Calcium carbonate; Magnesium slag

1. Introduction

With the rapid development of modern industry, anthropogenic carbon dioxide (CO_2) emissions have been exponentially increasing, posing a significant threat to the environment [1]. The cement industry, as a pillar of infrastructure development, is responsible

*CORRESPONDING AUTHOR:
Songhui Liu, Henan Key Laboratory of Materials on Deep-Earth Engineering, School of Materials Science and Engineering, Henan Polytechnic University, Jiaozuo, Henan, 454003, China; Email: liusonghui@hpu.edu.cn

ARTICLE INFO
Received: 19 November 2023 | Revised: 11 December 2023 | Accepted: 20 December 2023 | Published Online: 27 December 2023
DOI: https://doi.org/10.30564/jbms.v5i2.6092

CITATION
Ye, J.H., Liu, S.H., Fang, J.R., et al., 2023. Unveiling the Carbonation Behavior and Microstructural Changes of Magnesium Slag at 0 °C. Journal of Building Material Science. 5(2): 37-50. DOI: https://doi.org/10.30564/jbms.v5i2.6092

for approximately 7% of global CO_2 emissions [2]. The production of traditional Portland cement not only consumes massive amounts of raw materials and energy but also releases enormous amounts of CO_2 [3-5]. It is estimated that for every ton of Portland cement produced, approximately 0.8-1.0 tons of CO_2 are emitted. Consequently, developing alternative cementitious materials with low carbon footprints and CO_2 sequestration capacities has become an urgent need.

In recent years, mineral carbonation has emerged as a promising approach for reducing CO_2 emissions in the cement and construction sector [6-10]. This process chemically binds CO_2 with calcium or magnesium-rich materials to form stable carbonates, providing a route for permanent CO_2 sequestration [11-13]. Simultaneously, the carbonation reaction can produce supplementary cementitious materials (SCMs) with enhanced properties and reactivity [14,15]. Multiple industrial alkaline wastes and byproducts with high calcium or magnesium contents such as steel slags, power plant ashes, and magnesium slags have been identified as suitable precursors for mineral carbonation [16-20]. Compared to natural minerals, these artificial calcium/magnesium-rich solid wastes not only possess higher reactivity and faster carbonation kinetics but also allow for the recycling of industrial byproducts, enabling the realization of a cyclic economy [21-24].

Among various mineral carbonation options, the carbonation of magnesium slag has attracted increasing interest in recent years [25]. Magnesium slag is a byproduct of magnesium smelting processes, primarily consisting of calcium oxide (CaO), silicon dioxide (SiO_2), and magnesium oxide (MgO). With the dramatic growth in magnesium production, driven by strong market demand, China has become the world's largest magnesium producer, accounting for approximately 90% of the global output. Consequently, vast quantities of magnesium slag are being generated. Current estimates indicate an annual magnesium slag output of over 6 million tons in China. Despite its chemical composition rich in oxides, magnesium slag has found limited large-scale utilization due to issues such as low activity, poor stability, and potential expansion [26]. Landfilling has been the primary disposal route, leading to serious environmental problems and waste of resources.

The predominant mineral phase of magnesium slag is dicalcium silicate (C_2S), which exhibits high susceptibility to carbonation reactions [27-30]. Studies have confirmed that carbonation can effectively stimulate the hydration reactivity of C_2S while mitigating the expansion issues associated with magnesium slag [26]. Both dry and wet carbonation processes have been shown to improve the properties and activity of magnesium slag, transforming it into a viable SCM. Carbonated magnesium slag displays enhanced hydration activity, reduced CaO expansion, increased strength, and self-cementing characteristics when used as concrete admixtures. Moreover, accelerated carbonation curing has been successfully implemented to synthesize magnesium slag-based cementitious materials, with compressive strengths exceeding 100 MPa in some studies [31]. Evidently, carbonation provides an efficient technique to stabilize magnesium slag and unlock its latent hydraulic properties.

However, the carbonation of magnesium slag is a complex physicochemical process influenced by several parameters including CO_2 concentration, temperature, relative humidity, liquid/solid ratio, and pressure [26,32]. In particular, temperature plays a crucial role in shaping the carbonation reaction kinetics and the composition of reaction products [33]. Most studies have focused on investigating the effects of room temperature and elevated temperatures on the carbonation process [25]. Far fewer efforts have explored the implications of conducting carbonation under low-temperature conditions.

It is well established that temperature has a significant impact on the solubility of CO_2 as well as the dissolution kinetics of Ca^{2+} and Mg^{2+} ions, consequently affecting $CaCO_3$ crystallization and growth [34,35]. Lower temperatures lead to reduced CO_2 diffusion rates in the aqueous phase and hinder the dissolution of Ca^{2+} and Mg^{2+}, which directly controls the kinetics of calcium carbonate precipitation. Moreover, temperature influences the polymorphs

and morphology of the formed calcium carbonate crystals [36]. The effects of temperature on the carbonation reaction pathways and products are complex and remain incompletely understood.

Elucidating the implications of low-temperature carbonation on magnesium slag is important from both a scientific perspective, in terms of revealing the underlying mechanisms, as well as a practical viewpoint, in terms of assessing its potential for mitigating CO_2. Nevertheless, current literature lacks comprehensive investigations analyzing the phase transformations, microstructural changes, and CO_2 sequestration efficiency of magnesium slag undergoing carbonation specifically under low-temperature conditions. Most studies focus on room temperature or use elevated temperatures to accelerate the carbonation reactions. The carbonation behavior of magnesium slag at temperatures closer to natural conditions remains relatively unclear.

Therefore, this paper aims to conduct a detailed assessment of the effects of wet carbonation at 0 °C on the physiochemical characteristics of magnesium slag. The evolution of the phase composition at different carbonation conversion levels and its impacts on the microstructure, morphology, specific surface area, and porosity of magnesium slag will be analyzed using a suite of characterization techniques. The findings are expected to provide new insights into the implications of low-temperature environments on the carbonation mechanisms of magnesium slag. Furthermore, the results will allow evaluation of the CO_2 sequestration potential and the prospective utilization of magnesium slag as an SCM following low-temperature carbonation treatment.

2. Experimental program

2.1 Raw materials

The magnesium slag (MS) utilized in this study was acquired from Yulin City, Shanxi Province, China, employing the Pidgeon method. Deionized water sourced from the laboratory was employed as the solvent. The chemical composition of the magnesium slag and its particle size distribution are detailed in **Table 1** and **Figure 1**, respectively. The XRD of MS is shown in **Figure 2**.

Upon reviewing the data presented in **Table 1**, it is evident that the primary chemical constituents of MS are CaO, SiO_2, and MgO. Numerous studies have demonstrated that the elevated MgO content can result in later-stage matrix hydration expansion, thereby constraining the widespread utilization of MS [25,26]. However, the high content of Ca and Mg has very high carbonation activity, indicating that Pidgeon process magnesium slag does have great potential to sequester carbon dioxide.

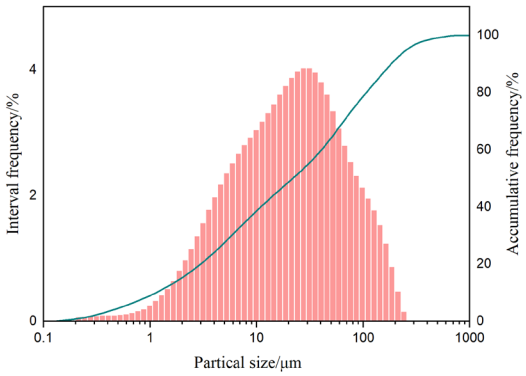

Figure 1. The particle size distribution of MS.

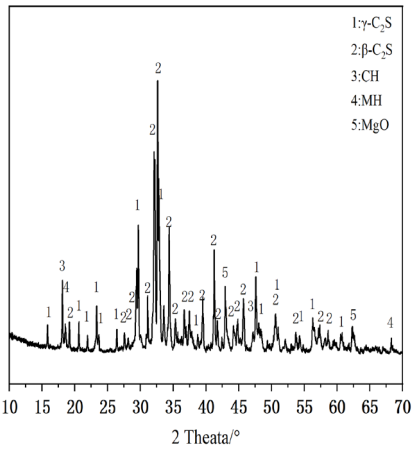

Figure 2. The XRD of MS.

Table 1. Chemical composition of MS.

Oxide	SiO_2	Al_2O_3	CaO	Fe_2O_3	MgO	Others
MS	29.88	1.06	50.98	3.52	11.27	3.29

2.2 The carbonation of MS

The carbonation of MS is shown in **Figure 3**. First,

the dried MS powder and chilled deionized water were weighed in the ratio of 1:40. Then, the suspension of MS and deionized water was placed into a large beaker containing ice cubes (size 10 × 10 × 10 mm^3) and cold deionized water. The speed of the stirring device was set to 400 r/min. To further dissolve the MS, the suspension was stirred for 10 min, and then carbon dioxide was injected into the suspension at a rate of 0.1 L/min/5 g of MS. Carbon dioxide was purchased from Gas Commerce at a concentration higher than 99.9%. The temperature of the MS suspension was monitored in real-time throughout the carbonation process using a temperature sensor. The temperature of the mass spectrometry suspension was maintained at around 0 °C by adjusting the amount of ice in the large beaker. Subsequently, the mass spectrometry suspensions of different carbonation times were vacuum filtered and the resulting samples were washed with anhydrous ethanol. This was done to ensure that the samples stopped hydrating and to facilitate drying. Finally, the samples were dried in a vacuum oven at 50 °C to obtain MS samples with different degrees of carbonation. The carbonated MS samples were named C-MS.

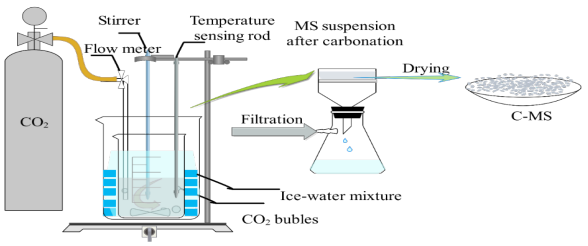

Figure 3. Preparation of C-MS powder samples.

2.3 Testing methods

X-ray diffractometer

The mineralogical composition of the samples was determined using an X-ray diffractometer equipped with a copper target (Rigaku, Tokyo, Japan). The test instrument utilizes an accelerating voltage of 45 kV and a current of 200 mA during the test. In addition, the instrument is set to analyze in 0.02 steps.

Thermal analysis

The comprehensive thermal analyzer (BJ-HCT-3) used in this study was produced by Beijing Hengjiu Scientific Instrument Factory. Before the test begins, the powder sample is weighed and placed on a sample stage. The instrument temperature is raised from room temperature to 1000 °C at a rate of 10 °C/min.

Fourier transform spectra (FTIR)

To further examine the development of the silicon phase present in the samples, an analysis was conducted using Fourier transform spectroscopy employing the solid powder total reflection method. The testing instrument employed was a fully automated switching Fourier transform spectrometer model V70, covering a range of 400 to 4000 cm^{-1} [25]. All powdered specimens were maintained in a dry and ground state for the analysis.

To further explore the ratio change of silica gel and C-S-H gel under different carbonation conditions, the spectrum between 1000 and 1200 cm^{-1} was deconvolved using Origin Pro software. According to the peak range of silica gel and C-S-H, the position of the target peak was determined, and the original curve was divided into C-S-H peak and silica gel peak, to clarify the process of MS carbonation products at low temperatures.

Scanning electron microscope (SEM)

Scanning electron microscope (SEM) images of the powder samples were obtained using a Merlin SEM in high vacuum mode at an accelerating voltage of 15 kV. To enhance conductivity, all samples were coated with a thin layer of gold.

Pore structure

In studying the evolution of pore structure in C-MS under varying degrees of carbonation, the TriStar II 3020BET tester from Micromeritics was employed [37]. The examination centered on assessing alterations in the total specific surface area and pore volume of the samples. Before the analysis, a degassing procedure was carried out on the samples at a temperature of 45 °C for 6 hours to eliminate any remaining moisture and gaseous impurities.

3. Results and discussion

3.1 Carbonation degree

Figure 4 depicts the TG-DTG curves of MS

with varying degrees of carbonation. A total of four different weight loss peaks can be seen in the DTG results. First, the weight loss peak near 100 °C is the loss of mass due to the evaporation of bound water from the amorphous gel in the sample. It is interesting to note that after 480 minutes of carbonation, the peak weight loss is highest at 100 °C, indicating that the largest amount of gel was produced at this time. The weight loss peak observed in the temperature range of 400-450 °C is attributed to the mass loss resulting from the thermal decomposition of calcium hydroxide ($Ca(OH)_2$), a hydration product, at high temperatures [38,39]. The weight loss peak observed in the temperature range of 500-600 °C is attributed to the de-carbonation processes of amorphous calcium carbonate (ACC) and poorly crystalline vaterite [40]. Furthermore, the weight loss peak observed between 700-800 °C is caused by the high-temperature decomposition of calcite [41]. Notably, this peak exhibits an increasing trend and gradually shifts to higher temperatures with prolonged carbonation.

The calcium carbonate content under various carbonation conditions was determined using Equation (1), while Equations (2)-(4) were utilized to calculate the degree of carbonation of MS at different carbonation times under an ambient temperature of 0 °C [42].

$$Cc(\%) = \frac{Cc_{CO_2} \times \left(\frac{100}{44}\right)}{M_{900°C}} * 100\% \quad (1)$$

$$\partial = \frac{CO_{2uptake.actual}}{CO_{2uptake.max}} \quad (2)$$

$$CO_{2uptake.actual} = \left(\frac{Cc_{CO_2}}{M_{900°C}}\right) \quad (3)$$

$$CO_{2uptake.max} = \left(\frac{M_{CO_2}}{M_{CaO}}\right) * [CaO + (1.09MgO)] \quad (4)$$

The CO_2 bound in $CaCO_3$ (550-850 °C) is represented by Cc_{CO2}, while $M_{900°C}$ denotes the residual mass at 900 °C. Additionally, M_{CO2} and M_{CaO} refer to the molecular weights of CO_2 and CaO, respectively. The MgO content of cement can be found in **Table 1**. The calculation results are shown in **Table 2**.

Figure 5 illustrates the variation of carbonation degree in MS at different carbonation times. The process can be divided into three stages. Firstly, during the initial ten minutes of carbonation reaction, the carbonation degree of MS increases from an initial 6% to 40%. In this stage, the dissolution rate of CO_2 in water becomes the determining factor. Subsequently, the carbonation reaction enters the second stage, where the carbonation process of MS is influenced by the dissolution and transfer rate of minerals and Ca^{2+} [42]. Compared to the first stage, the rate of carbonation degree advancement in MS slows down, with only a 30% increase after 50 minutes. As the carbonation reaction progresses to the third stage, the continuous low-temperature environment restricts the diffusion of CO_2 and the migration of Ca^{2+}, significantly prolonging the reactivity of the carbonation process [35,42]. It takes 480 minutes for the carbonation degree of MS to reach 80%.

From the above results, it can be observed that even when the carbonation reaction of MS continues in a low-temperature environment, the early-stage reactivity is primarily influenced by the dissolution of CO_2 and the migration of Ca^{2+}. It is not until the later stage of the carbonation reaction that the continuous low temperature imposes restrictive effects on the carbonation process in MS.

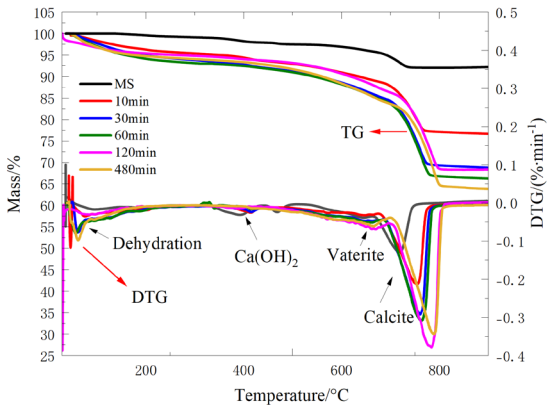

Figure 4. TG-DTG curves of MS with different carbonation times.

Table 2. The calculation results of MS under different carbonation times.

Time/min	Cc_{CO2}/%	CC%	α/%
0	5.30	13.07	6.8
10	15.23	45.18	40.11
30	21.25	70.16	61.72
60	23.40	80.35	70.55
120	23.91	79.52	70.57
480	26.22	93.30	83.23

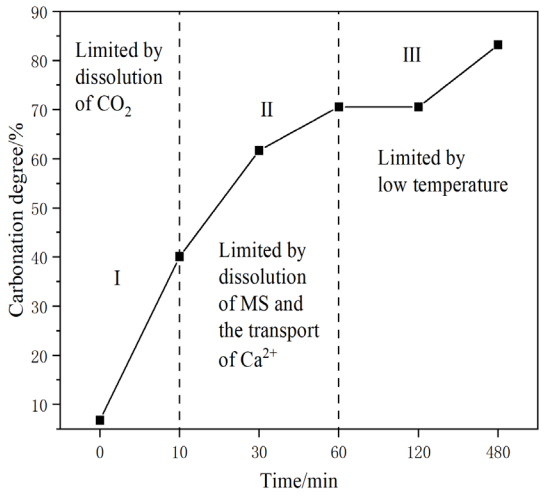

Figure 5. Carbonation degree of MS with different carbonation times.

3.2 Phase composition

Figure 6 presents the XRD analysis of MS with different carbonation times under low-temperature conditions. In **Figure 6**, it is observed that the predominant carbonation product of MS at low temperatures is calcite. The position of the calcite diffraction peak remains relatively unchanged with increasing carbonation time, but its intensity increases, leading to a weakening of the C_2S diffraction peak. This phenomenon arises from the continuous injection of carbon dioxide, which dissolves in water, generating carbonic acid. The carbonic acid subsequently reacts with the dissolved Ca^{2+} ions present in the mineral suspension, resulting in the precipitation of calcite. Consequently, the presence of calcite leads to an observable increase in the diffraction peak associated with its crystal structure. Additionally, faint calcite diffraction peaks are also noticeable in the XRD curves of the uncarbonated MS, indicating a minor carbonation reaction of the material.

According to the XRD results, the main carbonated products of MS were not affected under prolonged low-temperature conditions. In the early stage of the carbonation reaction (10-30 minutes), the diffraction peak of the C_2S mineral gradually weakened, while the diffraction peak belonging to calcite gradually increased, and a weak peak of vaterite also appeared. This indicates that temperature does not have a significant influence on the products in the early stage of wet carbonation, and the post-carbonated products of MS still exist predominantly in the crystalline form of calcite. As the carbonation reaction enters the intermediate stage (30-60 minutes), the number of calcite diffraction peaks increases and the peak intensity gradually increases, while the vaterite diffraction peak becomes more pronounced. With the extension of carbonation time, the diffraction peak of C_2S eventually disappears. When the carbonation time reaches 480 minutes, the peak intensity of calcite reaches its maximum. These results show that the early stage (30 min) of the carbonation reaction at a low temperature helps to stabilize the crystal structure of vaterite, but as the carbonation reaction continues, the vaterite transforms into calcite.

Numerous studies have shown that the crystal forms of calcium carbonate are mainly divided into three types, namely calcite, aragonite, and vaterite, in the order of increasing stability. Among them, vaterite easily transforms into calcite in aqueous solutions. From the results in **Figure 6**, it can be observed that the low-temperature environment contributes to stabilizing the crystal structure of vaterite. This phenomenon can be attributed to the fact that low temperature restricts the diffusion of CO_2 gas in the aqueous solution and the migration of Ca^{2+}, thereby impeding the transformation process of vaterite to calcite and allowing vaterite to exist stably [35].

3.3 Evolution of Si

Figure 7 displays the FTIR spectra, revealing absorption bands associated with ACC (amorphous calcium carbonate) and calcite. Based on the results, a total of four vibrational peaks were observed. Specifically, the peaks observed at 1417 cm^{-1} and 712 cm^{-1} correspond to the asymmetric stretching vibration (υ^3) and in-plane bending vibration (υ^2) of the C-O bond, respectively [43]. Additionally, the peak at 868 cm^{-1}

represents the out-of-plane bending vibration (υ^4) of the C-O bond. These findings once again confirm the presence of carbonates. It is noteworthy that the vibrational peaks observed in the wavenumber range of 993-1066 cm^{-1} represent the vibration of the Si-O bond (υ^3). This indicates that after undergoing carbonation at 0 °C, the silicon in MS exists in the form of highly polymerized silica gel.

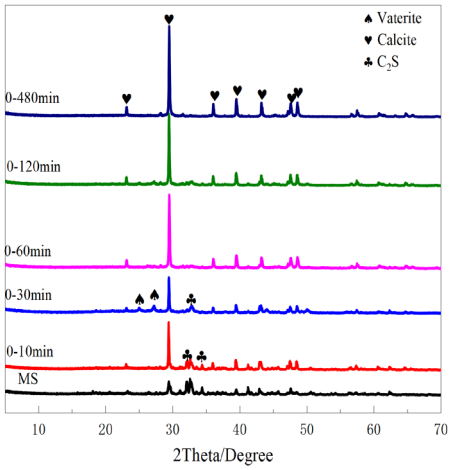

Figure 6. XRD analysis of MS with different carbonation times under low-temperature conditions.

Similar to the XRD results, faint vibrational peaks related to calcite are observed in the FTIR analysis of the uncarbonated MS, providing further evidence of slight carbonation. With the progression of the reaction, an increase in the amount of calcite is observed. Notably, the vibrational peak of the Si-O bond shifts to a higher wave number (1066 cm^{-1}), indicating an enhanced degree of polymerization of the silica-oxygen tetrahedra and the formation of highly polymerized silica gel. This transition becomes more apparent after 30 minutes of carbonation, consistent with our previous findings suggesting a significant enhancement in the degree of polymerization of gel products generated from MS, both at room temperature and under low-temperature conditions.

To gain a better understanding of the evolution of silicon dioxide phase structures in MS during carbonation, the vibrational peaks between 800 cm^{-1} and 1200 cm^{-1} were analyzed for samples with different carbonation times (As shown in **Figure 8**). Previous studies have demonstrated the feasibility of using FTIR analysis to determine the levels of unhydrated phases, hydrated calcium silicate gel (C-S-H), and silica gel [42]. The fitting results are shown in **Table 3**.

The results indicate that during carbonation reactions conducted in a low-temperature environment, prior to 30 minutes of carbonation time, decalcification of hydrated calcium silicate gel and an increase in silica gel content were observed. As the carbonation reaction continued for 120 minutes, further decalcification of hydrated calcium silicate gel occurred, leading to its conversion into silica gel and resulting in an increased silica gel content.

These findings reveal that a sustained low-temperature environment does not significantly influence the transformation of early gel products during the carbonation of MS. After 120 minutes, although the continuous low-temperature environment limits the diffusion of CO_2 and the migration of Ca^{2+}, it actually facilitates the inward progress of the carbonation reaction, thereby increasing the degree of carbonation and the silica gel content within the matrix [35].

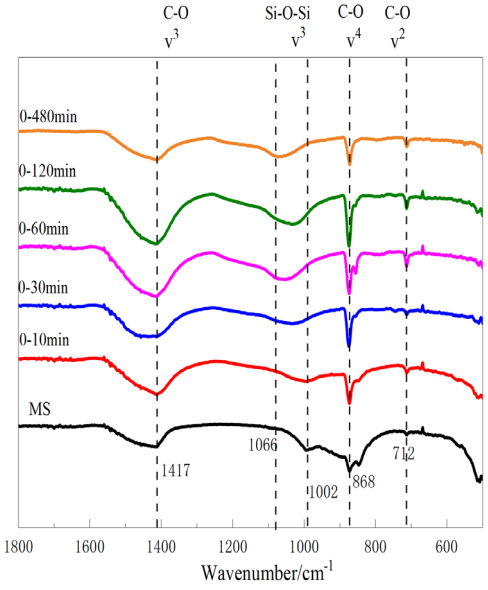

Figure 7. FTIR analysis of MS with different carbonation times under low-temperature conditions.

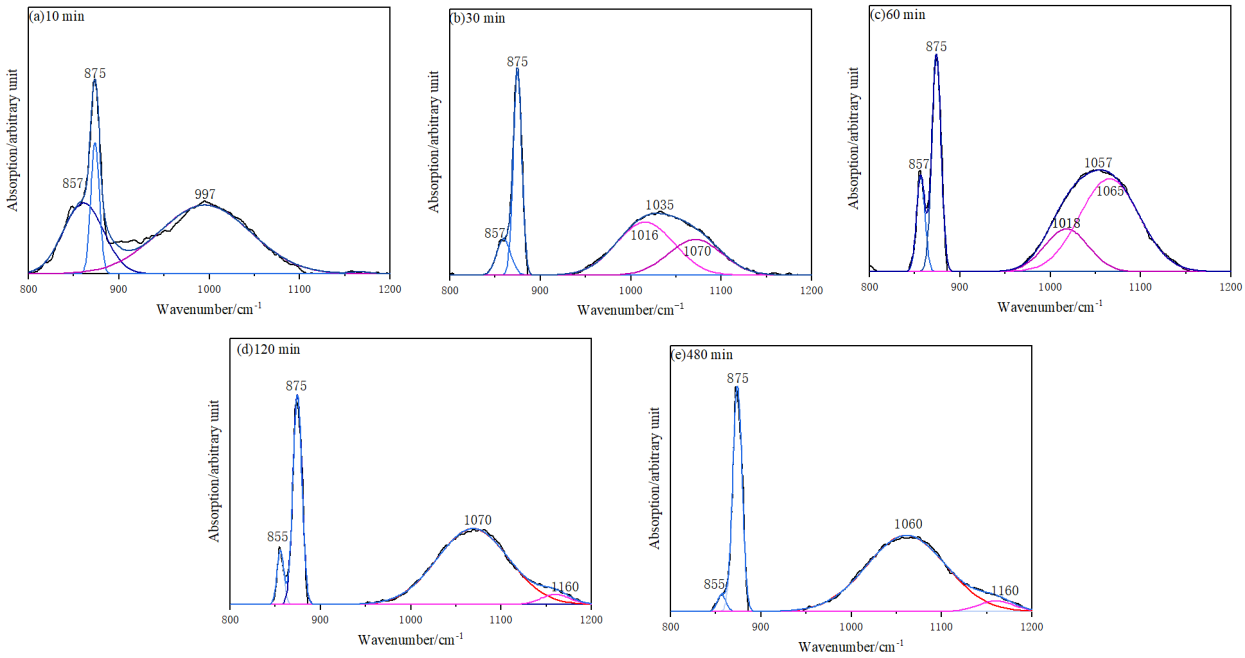

Figure 8. The resolving of the overlapping peak of FTIR spectra between 800 and 1200 cm^{-1} of carbonated MS samples at different carbonation conditions (a) 10 min, (b) 30 min, (c) 60 min, (d) 120 min and (e) 480 min.

Table 3. The deconvolution results of FTIR curves between 800 and 1200 cm^{-1} (%).

Time/min	Unhydrated phases	C-S-H gel	Silica gel
10	30.91%	68.73%	0.36%
30	9.25%	55.66%	35.09%
60	11.86%	22.71%	65.43%
120	8.08%	0	91.92%
480	5.31%	0	94.69%

3.4 Microstructure of C-MS

SEM

Figure 9 presents the SEM-EDS images of C-MS. By comparing the microscopic morphology of MS with different carbonation degrees, several important observations can be made.

In just 10 minutes, the carbonation reaction yields calcite with distinct morphology, indicating the rapid nature of the carbonation process even at low temperatures. At 30 minutes, ACC gradually transforms into vaterite. At this point, most of the calcite and vaterite are 0.8 μm in size, with only a few vaterites reaching 1.5 μm in diameter. In addition, small-sized calcite particles begin to aggregate, forming rhombic massive calcite structures with a large number of vaterite particles and gel products attached. The produced calcite and vaterite particles have sizes not exceeding 1 μm. As the carbonation reaction progresses (between 60-120 minutes), the calcite particles become tightly surrounded by a significant amount of gel products. This phenomenon becomes even more pronounced at the 480-minute.

Compared to previous studies, when wet carbonation of MS is conducted at room temperature, the resulting calcium carbonate exists in the forms of calcite and aragonite, with calcite being dominant. However, under low-temperature conditions, the aragonite form of calcium carbonate disappears, and a larger quantity of vaterite appears. Additionally, from **Figure 9(b)**, it can be observed that the calcite formed under low-temperature conditions adopts a cubic structure, while vaterite has a more complete

spherical shape. The reason for this phenomenon is that prolonged low-temperature conditions restrict the diffusion rate of CO_2 gas in the aqueous solution, but promote internal carbonation, resulting in more complete carbonation of the matrix and complete growth of calcite crystals. Furthermore, low temperature hinders the migration of Ca^{2+} dissolved from minerals like C_2S, limiting the nucleation process of calcium carbonate and the transformation of vaterite into calcite. As a result, the layered calcite structure disappears, and well-formed cubic calcite crystals emerge.

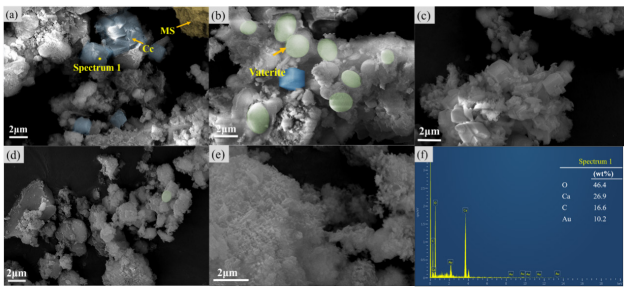

Figure 9. SEM-EDS images of C-MS: (a) 10 min; (b) 30 min; (c) 60 min; (d) 120 min; (e) 480 min; (f) EDS of the spectrum.

BET surface area and pore structure

To investigate the changes in MS pore structure under low-temperature conditions at different degrees of carbonation, the BET analysis method was employed in this study. **Figures 10(a) and 10(b)** present the N_2 adsorption isotherm plots and pore volume distribution of MS with varying degrees of carbonation. **Figure 10(a)** reveals a significant increase in nitrogen uptake when the carbonation time reaches 30 minutes and the relative pressure ranges from 0.7 to 1. The uptake experiences a sharp increase at 120 minutes, accompanied by an expanded relative pressure range. Additionally, **Figure 10(b)** provides further insights into the pore size distribution of MS.

The BET test results of MS with different carbonation degrees are listed in **Table 4**. From the results, it can be seen that the hole volume and specific surface area of MS gradually increase with the increase of carbonation degree. However, there is a slight decrease in specific surface area at 10 and 60 minutes. A comparison of MS test results before and after 120 minutes of carbonation showed a significant increase in the cumulative pore volume, from 0.024245 cm^3/g to 0.047098 cm^3/g. This observed increase can be attributed to the continued dissolution of minerals present in the MS during the decalcification process, especially C_2S. As a result, a significant change in the phase composition of the MS occurs, leading to an increase in the pore volume. In addition, **Figure 10(b)** shows a clear trend of increasing volume of pores larger than 25 nm as well as gel pores smaller than 25 nm. This trend can be attributed to the formation of van der Waals and hydrogen bonds during carbonation [37]. Consequently, this leads to an increase in the number of small particles and pores, which ultimately results in an overall increase in pore volume.

Based on our previous study and the FTIR analysis results (**Figure 7**), it is evident that gel polymerization begins after 30 minutes of carbonation. Consistently, the BET test results of MS also reveal an elevation in pore volume by approximately 73.7% after 30 minutes compared to uncarbonated MS. This can be attributed to the continuous dissolution of Ca^{2+}, which generates numerous fine pores and leads to the observed increase. After 480 min, it was found from the results that the specific surface area of MS increased by 740% and the pore volume increased by 144.6% compared with that before carbonation, which indicated a significant increase in the activity and specific surface area of MS during the low-temperature carbonation process.

3.5 Growth mechanism of CaCO3 under a low-temperature environment

This study investigates the carbonation behavior of MS at varying degrees under a low-temperature environment using XRD, TG, FTIR, BET, and SEM-EDS analysis. Based on the results of the above tests, it can be observed that the main carbonation products resulting from wet carbonation of MS at 0 °C are calcite and highly polymerized silica gel. **Figure 11** illustrates the evolution of $CaCO_3$ growth at low temperatures.

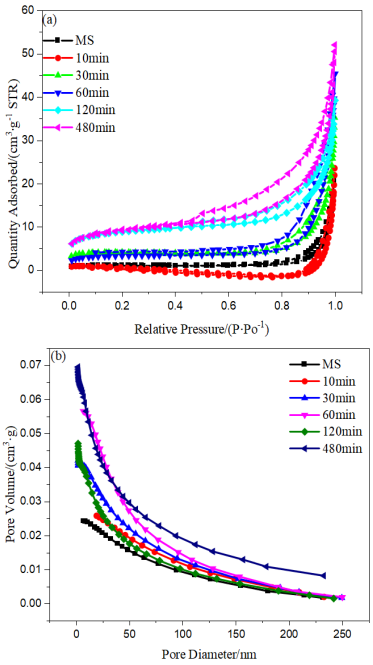

Figure 10. BET curves of MS with different degrees of carbonation.

Table 4. BET test results of MS with different degrees of carbonation.

Different time (min)	Specific surface area (m^2/g)	Hole volume (cm^3/g)
MS	3.5305	0.024245
10 min	1.1851	0.025903
30 min	12.8038	0.042108
60 min	10.4350	0.056580
120 min	28.9021	0.047098
480 min	29.6573	0.059295

In the initial stage (0-30 min), the carbonation reaction occurs rapidly, leading to the conversion of ACC into calcite. Calcite particles rapidly increase in size, while a small amount of silica-gel forms around them. Subsequently, after 30 minutes, the reaction enters the stabilization stage, and calcite decomposes into clusters of poorly crystallized and lumpy calcite due to cracking. The persistent low-temperature environment restricts the diffusion rate of CO_2 and the dissolution of Ca^{2+} and Mg^{2+}, thereby influencing the growth of calcite crystals. Additionally, vaterite, derived from ACC, surrounds the calcite particles. In the final stage of the reaction, the low-temperature environment further hinders the growth rate of calcite particles, leading to the appearance of a gel layer on their surface.

The primary mineral component of MS, C_2S, is subject to various influential factors including Ca^{2+} ion concentration, ion leaching rate, and solution pH. These factors play a crucial role in determining the nucleation and growth processes of calcium carbonate. Compared to our previous studies on room-temperature wet carbonation, the main carbonation products observed at low temperatures consist of calcite crystals and highly polymerized gel structures, with significant gel polymerization occurring only at the 30-minute mark [25]. Notably, in contrast to the appearance of small amounts of aragonite in the carbonation products at room temperature, the low-temperature carbonation process does not generate aragonite, but rather small vaterite. Furthermore, it is worth noting that the amount of calcium carbonate generated during the same time frame at room temperature exhibits a substantial increase compared to that produced during low-temperature wet carbonation. This disparity suggests that the low-temperature environment significantly retards the rate of the carbonation reaction. Furthermore, the microscopic morphology of calcite at room temperature reveals a laminar accumulation with a small amount of aragonite and gel surrounding it, while calcite clusters generated at low temperatures exhibit a substantial presence of gel layers around them. In this study, the low-temperature carbonation process significantly limits the dissolution rate of Ca^{2+} ions, resulting in a lower concentration of Ca^{2+} ions in the MS suspension and a reduced carbonation rate for the corresponding minerals [35]. As a result, the production and size growth of calcite-type calcium carbonate is constrained.

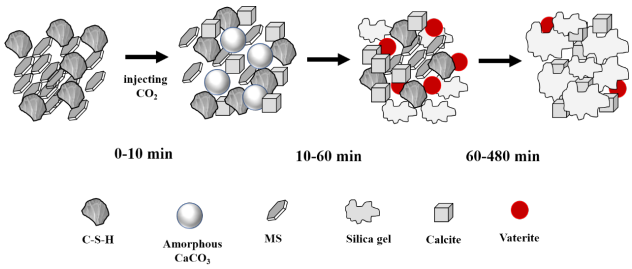

Figure 11. Evolution of $CaCO_3$ growth in a low-temperature environment.

4. Conclusions

This study investigated the carbonation behavior and microstructural changes of magnesium slag undergoing wet carbonation at 0 °C through a comprehensive set of characterization techniques. The following conclusions can be drawn:

(1) The predominant carbonation products are calcite, vaterite, and highly polymerized silica gel, with particle sizes around 1 μm. The persistent low-temperature environment affects the morphology and crystallization of calcium carbonate, slowing down the reaction kinetics.

(2) As carbonation progresses, a layer of silica gel envelops the surfaces of the formed calcium carbonate particles. The low temperature restricts the dissolution of Ca^{2+} ions, limiting the growth of calcite crystals.

(3) After 480 min of carbonation, the specific surface area and porosity of magnesium slag increased remarkably by 740% and 144.6%, respectively, indicating significantly improved reactivity and ultrafine particle size distribution

(4) The microstructure of carbonated magnesium slag became denser, with calcite particles intimately surrounded by the silica gel phase, due to the low temperature impeding crystal growth.

(5) Wet carbonation treatment at 0 °C can effectively transform magnesium slag into an ultrafine supplementary cementitious material with high CO_2 sequestration capacity.

Overall, this study provides new insights into the effects of low-temperature carbonation environments on the physicochemical characteristics of magnesium slag. The results demonstrate that wet carbonation at 0 °C significantly enhances the properties of magnesium slag, creating a high reactivity SCM product with major implications for reducing the carbon footprint of the cement and construction industry. Further research can build on these findings to optimize the synthesis conditions and expand the utility of carbonated magnesium slag.

Conflict of Interest

There is no conflict of interest.

Data Availability Statement

Data will be made available on request.

Acknowledgement

The authors appreciate the support from the National Key R & D Program Intergovernmental International Science and Technology Innovation Cooperation Project (2018YFE0107300), the China Building Materials Federation (20221JBGS03-11), the Science and Technology Project of Henan Province (211110231400, 212102310559, 212102310564, 222300420167, 22A430022), the Opening Project of the State Key Laboratory of Green Building Materials (2021GBM06), the Henan Outstanding Foreign Scientists' Workroom (GZS2021003).

References

[1] Zajac, M., Song, J., Ullrich, P., et al., 2024. High early pozzolanic reactivity of alumina-silica gel: A study of the hydration of composite cements with carbonated recycled concrete paste. Cement and Concrete Research. 175, 107345. DOI: https://doi.org/10.1016/j.cemconres.2023.107345

[2] Liu, Z., Lv, C., Wang, F., et al., 2023. Recent advances in carbonatable binders. Cement and Concrete Research. 173, 107286. DOI: https://doi.org/10.1016/j.cemconres.2023.107286

[3] Poon, C.S., Shen, P., Jiang, Y., et al., 2023. Total recycling of concrete waste using accelerated carbonation: A review. Cement and Concrete Research. 173, 107284. DOI: https://doi.org/10.1016/j.cemconres.2023.107284

[4] Cui, K., Lau, D., Zhang, Y., et al., 2021. Mechanical properties and mechanism of nano-Ca-

CO_3 enhanced sulphoaluminate cement-based reactive powder concrete. Construction and Building Materials. 309, 125099.
DOI: https://doi.org/10.1016/j.conbuildmat.2021.125099

[5] Shang, D., Wang, M., Xia, Z., et al., 2017. Incorporation mechanism of titanium in Portland cement clinker and its effects on hydration properties. Construction and Building Materials. 146, 344-349.
DOI: https://doi.org/10.1016/j.conbuildmat.2017.03.129

[6] Mao, Y., Drissi, S., He, P., et al., 2024. Quantifying the effects of wet carbonated recycled cement paste powder on the properties of cement paste. Cement and Concrete Research. 175, 107381.
DOI: https://doi.org/10.1016/j.cemconres.2023.107381

[7] Jiang, Y., Li, L., Lu, J.X., et al., 2022. Mechanism of carbonating recycled concrete fines in aqueous environment: The particle size effect. Cement and Concrete Composites. 133, 104655.
DOI: https://doi.org/10.1016/j.cemconcomp.2022.104655

[8] Chang, J., Xiong, C., Zhang, Y., et al., 2019. Foaming characteristics and microstructure of aerated steel slag block prepared by accelerated carbonation. Construction and Building Materials. 209, 222-233.
DOI: https://doi.org/10.1016/j.conbuildmat.2019.03.077

[9] Liu, S., Dou, Z., Zhang, S., et al., 2017. Effect of sodium hydroxide on the carbonation behavior of β-dicalcium silicate. Construction and Building Materials. 150, 591-594.
DOI: https://doi.org/10.1016/j.conbuildmat.2017.04.145

[10] Fang, Y., Chang, J., 2015. Microstructure changes of waste hydrated cement paste induced by accelerated carbonation. Construction and Building Materials. 76, 360-365.
DOI: https://doi.org/10.1016/j.conbuildmat.2014.12.017

[11] Li, W., Cao, M., Wang, D., et al., 2023. Improving the hydration activity and volume stability of the RO phases in steel slag by combining alkali and wet carbonation treatments. Cement and Concrete Research. 172, 107236.
DOI: https://doi.org/10.1016/j.cemconres.2023.107236

[12] Mo, L., Yang, S., Huang, B., et al., 2020. Preparation, microstructure and property of carbonated artificial steel slag aggregate used in concrete. Cement and Concrete Composites. 113, 103715.
DOI: https://doi.org/10.1016/j.cemconcomp.2020.103715

[13] Qu, M., Liu, P., Zhao, D., et al., 2020. CO_2 capture and conversion by an organosilane-modified cementitious material. Construction and Building Materials. 253, 119198.
DOI: https://doi.org/10.1016/j.conbuildmat.2020.119198

[14] Zajac, M., Skocek, J., Gołek, Ł., et al., 2023. Supplementary cementitious materials based on recycled concrete paste. Journal of Cleaner Production. 387, 135743.
DOI: https://doi.org/10.1016/j.jclepro.2022.135743

[15] Liu, P., Zhong, J., Zhang, M., et al., 2021. Effect of CO_2 treatment on the microstructure and properties of steel slag supplementary cementitous materials. Construction and Building Materials. 309, 125171.
DOI: https://doi.org/10.1016/j.conbuildmat.2021.125171

[16] Liu, P., Mo, L., Zhang, Z., 2023. Effects of carbonation degree on the hydration reactivity of steel slag in cement-based materials. Construction and Building Materials. 370, 130653.
DOI: https://doi.org/10.1016/j.conbuildmat.2023.130653

[17] Lu, B., Zhou, Y., Jiang, L., et al., 2024. High-purity vaterite $CaCO_3$ recovery through wet carbonation of magnesium slag and leaching residue utilization in cement. Cement and Concrete Composites. 145, 105353.

DOI: https://doi.org/10.1016/j.cemconcomp.2023.105353

[18] Liu, P., Zhang, M., Mo, L., et al., 2022. Probe into carbonation mechanism of steel slag via FIB-TEM: The roles of various mineral phases. Cement and Concrete Research. 162, 106991. DOI: https://doi.org/10.1016/j.cemconres.2022.106991

[19] Chang, J., Gu, Y., Ansari, W.S., 2020. Mechanism of blended steel slag mortar with CO_2 curing exposed to sulfate attack. Construction and Building Materials. 251, 118880. DOI: https://doi.org/10.1016/j.conbuildmat.2020.118880

[20] Mo, L., Zhang, F., Panesar, D.K., et al., 2017. Development of low-carbon cementitious materials via carbonating Portland cement-fly ash-magnesia blends under various curing scenarios: A comparative study. Journal of Cleaner Production. 163, 252-261. DOI: https://doi.org/10.1016/j.jclepro.2016.01.066

[21] Liu, S., Pan, C., Zhang, H., et al., 2023. Development of novel mineral admixtures for sulphoaluminate cement clinker: The effects of wet carbonation activated red mud. Journal of Building Engineering. 67, 105920. DOI: https://doi.org/10.1016/j.jobe.2023.105920

[22] Jiang, Y., Li, L., Lu, J.X., et al., 2022. Enhancing the microstructure and surface texture of recycled concrete fine aggregate via magnesium-modified carbonation. Cement and Concrete Research. 162, 106967. DOI: https://doi.org/10.1016/j.cemconres.2022.106967

[23] Zhang, W., Luan, Z., Ren, X., et al., 2022. Influence of alumina modulus on formation of high-magnesium clinker and morphological evolution of MgO. Cement and Concrete Research. 162, 106986. DOI: https://doi.org/10.1016/j.cemconres.2022.106986

[24] Mo, L., Panesar, D.K., 2012. Effects of accelerated carbonation on the microstructure of Portland cement pastes containing reactive MgO. Cement and Concrete Research. 42(6), 769-777. DOI: https://doi.org/10.1016/j.cemconres.2012.02.017

[25] Ye, J., Liu, S., Zhao, Y., et al., 2023. Development of ultrafine mineral admixture from magnesium slag and sequestration of CO_2. Buildings. 13(1), 204. DOI: https://doi.org/10.3390/buildings13010204

[26] Zhang, C., Liu, S., Tang, P., et al., 2023. Enhancing the hardening properties and microstructure of magnesium slag blocks by carbonation-hydration sequential curing. Journal of Building Engineering. 76, 107414. DOI: https://doi.org/10.1016/j.jobe.2023.107414

[27] Zhang, C., Liu, S., Luo, S., et al., 2022. Effects of sodium doping on carbonation behavior of α-CS. Cement and Concrete Composites. 131, 104607. DOI: https://doi.org/10.1016/j.cemconcomp.2022.104607

[28] Zhao, S., Liu, Z., Mu, Y., et al., 2020. Effect of chitosan on the carbonation behavior of γ-C2S. Cement and Concrete Composites. 111, 103637. DOI: https://doi.org/10.1016/j.cemconcomp.2020.103637

[29] Wang, D., Chang, J., 2019. Comparison on accelerated carbonation of β-C_2S, $Ca(OH)_2$, and C_4AF: Reaction degree, multi-properties, and products. Construction and Building Materials. 224, 336-347. DOI: https://doi.org/10.1016/j.conbuildmat.2019.07.056

[30] Mu, Y., Liu, Z., Wang, F., et al., 2018. Effect of barium doping on carbonation behavior of γ-C_2S. Journal of CO_2 Utilization. 27, 405-413. DOI: https://doi.org/10.1016/j.jcou.2018.08.018

[31] Mo, L., Hao, Y., Liu, Y., et al., 2019. Preparation of calcium carbonate binders via CO_2 activation of magnesium slag. Cement and Concrete Research. 121, 81-90. DOI: https://doi.org/10.1016/j.cemconres.2019.04.005

[32] Tan, Y., Liu, Z., Wang, F., 2022. Effect of tem-

perature on the carbonation behavior of γ-C_2S compacts. Cement and Concrete Composites. 133, 104652.
DOI: https://doi.org/10.1016/j.cemconcomp.2022.104652

[33] Luo, Z., Wang, Y., Yang, G., et al., 2021. Effect of curing temperature on carbonation behavior of steel slag compacts. Construction and Building Materials. 291, 123369.
DOI: https://doi.org/10.1016/j.conbuildmat.2021.123369

[34] Wasylenki, L.E., Dove, P.M., De Yoreo, J.J., 2005. Effects of temperature and transport conditions on calcite growth in the presence of Mg^{2+}: Implications for paleothermometry. Geochimica et Cosmochimica Acta. 69(17), 4227-4236.
DOI: https://doi.org/10.1016/j.gca.2005.04.006

[35] Xu, Z., Zhang, Z., Huang, J., et al., 2022. Effects of temperature, humidity and CO_2 concentration on carbonation of cement-based materials: A review. Construction and Building Materials. 346, 128399.
DOI: https://doi.org/10.1016/j.conbuildmat.2022.128399

[36] Liendo, F., Arduino, M., Deorsola, F.A., et al., 2022. Factors controlling and influencing polymorphism, morphology and size of calcium carbonate synthesized through the carbonation route: A review. Powder Technology. 398, 117050.
DOI: https://doi.org/10.1016/j.powtec.2021.117050

[37] Liu, S., Shen, Y., Wang, Y., et al., 2022. Upcycling sintering red mud waste for novel superfine composite mineral admixture and CO_2 sequestration. Cement and Concrete Composites. 129, 104497.
DOI: https://doi.org/10.1016/j.cemconcomp.2022.104497

[38] Li, H., Liu, Y., Yang, K., et al., 2022. Effects of synthetic CSH-tartaric acid nanocomposites on the properties of ordinary Portland cement. Cement and Concrete Composites. 129, 104466.
DOI: https://doi.org/10.1016/j.cemconcomp.2022.104466

[39] Xue, J., Liu, S., Ma, X., et al., 2022. Effect of different gypsum dosage on the chloride binding properties of C_4AF hydrated paste. Construction and Building Materials. 315, 125562.
DOI: https://doi.org/10.1016/j.conbuildmat.2021.125562

[40] Shen, P., Zhang, Y., Jiang, Y., et al., 2022. Phase assemblance evolution during wet carbonation of recycled concrete fines. Cement and Concrete Research. 154, 106733.
DOI: https://doi.org/10.1016/j.cemconres.2022.106733

[41] Liu, S., Shen, Y., Wang, Y., et al., 2021. Synergistic use of sodium bicarbonate and aluminum sulfate to enhance the hydration and hardening properties of Portland cement paste. Construction and Building Materials. 299, 124248.
DOI: https://doi.org/10.1016/j.conbuildmat.2021.124248

[42] Mao, Y., He, P., Drissi, S., et al., 2023. Effect of conditions on wet carbonation products of recycled cement paste powder. Cement and Concrete Composites. 144, 105307.
DOI: https://doi.org/10.1016/j.cemconcomp.2023.105307

[43] Shen, P., Lu, J., Zhang, Y., et al., 2022. Preparation aragonite whisker-rich materials by wet carbonation of cement: Towards yielding micro-fiber reinforced cement and sequestrating CO_2. Cement and Concrete Research. 159, 106891.
DOI: https://doi.org/10.1016/j.cemconres.2022.106891